
Hierarchical Disentangled Representations

Babak Esmaeili

Northeastern University
esmaeili.b@husky.neu.edu

Hao Wu

Northeastern University
wu.hao10@husky.neu.edu

Sarthak Jain

Northeastern University
jain.sar@husky.neu.edu

Siddharth Narayanaswamy

University of Oxford
nsid@robots.ox.ac.uk

Brooks Paige

Alan Turing Institute
University of Cambridge
bpaige@turing.ac.uk

Jan-Willem van de Meent

Northeastern University
j.vandemeent@northeastern.edu

Abstract

Deep latent-variable models learn representations of high-dimensional data in an unsupervised manner. A number of recent efforts have focused on learning representations that disentangle statistically independent axes of variation, often by introducing suitable modifications of the objective function. We synthesize this growing body of literature by formulating a generalization of the evidence lower bound that explicitly represents the trade-offs between sparsity of the latent code, bijectivity of representations, and coverage of the support of the empirical data distribution. Our objective is also suitable to learning hierarchical representations that disentangle blocks of variables whilst allowing for some degree of correlations within blocks. Experiments on a range of datasets demonstrate that learned representations contain interpretable features, are able to learn discrete attributes, and generalize to unseen combinations of factors.

1 Introduction

Deep generative models represent data \mathbf{x} using a low-dimensional set of latent variables \mathbf{z} (sometimes referred to as a code). The relationship between \mathbf{x} and \mathbf{z} is described by a conditional probability distribution $p_\theta(\mathbf{x}|\mathbf{z})$ parameterized by a deep neural network. These models have seen much recent success in training generative models that can simulate high-fidelity representations of complex data such as images [Gatys et al., 2015; Gulrajani et al., 2017], audio [Oord et al., 2016], and language [Bowman et al., 2016]. The smooth low-dimensional \mathbf{z}

can be used as a compressed representation for downstream tasks such as text classification [Xu et al., 2017], Bayesian optimization [Gómez-Bombarelli et al., 2018; Kusner et al., 2017], and lossy image compression [Theis et al., 2017]. The setting in which an approximate posterior distribution $q_\phi(\mathbf{z}|\mathbf{x})$ is learned simultaneously to the generative model is known as a variational autoencoder (VAE), where $q_\phi(\mathbf{z}|\mathbf{x})$ and $p_\theta(\mathbf{x}|\mathbf{z})$ represent probabilistic encoders and decoders respectively.

While deep generative models often provide high-fidelity reconstructions, the representation \mathbf{z} is generally not directly amenable to human interpretation. In contrast to classical linear methods such as principal component or factor analysis, individual dimensions of \mathbf{z} do not necessarily encode any particular semantically meaningful variation in \mathbf{x} . This has motivated a search for ways of learning *disentangled* representations, where perturbations of individual dimensions of a the latent code \mathbf{z} perturb the corresponding \mathbf{x} in an interpretable manner.

Recent work in learning disentangled representations using deep generative models has broadly followed two approaches, one (semi-)supervised and one unsupervised. In the supervised or semi-supervised setting, a generative model is specified which allows for inclusion of prior information on what may constitute a factor of variation. This supervision may take the form of partitioning the data into subsets which vary only along some particular qualitative dimension [Kulkarni et al., 2015; Bouchacourt et al., 2017], or may take the form of explicit labels of particular sources of variation for some or all of the data [Kingma et al., 2014; Siddharth et al., 2017]. In this latter work, the overall training objective is largely kept the same, and instead the focus is on defining structured VAEs [Johnson et al., 2016] that incorporating a graphical model structure which partitions the latent variables \mathbf{z} into interpretable and uninterpretable subsets of dimen-

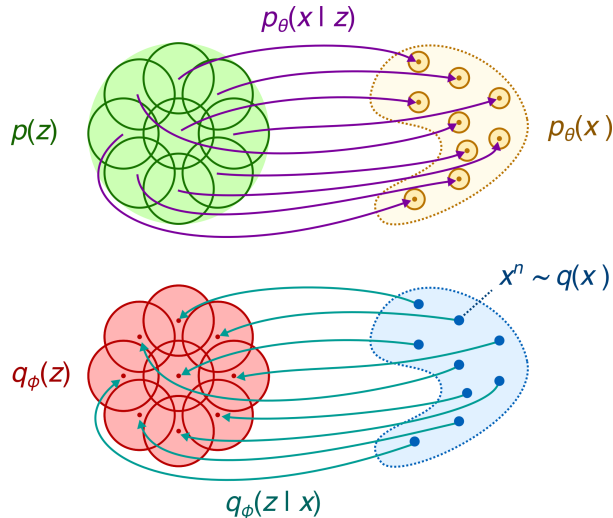


Figure 1: Correspondence between the generative model $p_\theta(\mathbf{x}, \mathbf{z})$ and the inference model $q_\phi(\mathbf{z}, \mathbf{x})$ in variational autoencoders. The generative model combines a prior $p(\mathbf{z})$ over latent variables with a likelihood $p_\theta(\mathbf{x} | \mathbf{z})$. In the inference model, a distribution $q(\mathbf{x})$ over a finite sample set approximates an unknown data distribution. The VAE objective minimizes the KL divergence between $q_\phi(\mathbf{z}, \mathbf{x})$ and $p_\theta(\mathbf{x}, \mathbf{z})$, which means that the inference marginal $q_\phi(\mathbf{z})$ must match the prior, the generative marginal $p_\theta(\mathbf{x})$ must match the empirical data distribution $q(\mathbf{x})$, and the generative posterior $p_\theta(\mathbf{x} | \mathbf{z})$ must match the encoder distribution $q_\phi(\mathbf{z} | \mathbf{x})$.

sions, and makes explicit any hierarchical or structured relationship between these latent variables.

In contrast, unsupervised methods for learning disentangled factors don’t require specification of which aspects of variation in the data we may wish to extract. Instead, these methods modify the objective function, penalizing specific terms in order to induce representations in which latent variables naturally coincide with preconceived notions of disentangled factors. The β -VAE [Higgins et al., 2016] modifies the VAE objective to encourage independence between the dimensions of the latent \mathbf{z} . Three recent papers [Kim and Mnih, 2018; Gao et al., 2018; Chen et al., 2018] all aim to address limitations of the β -VAE by specifically focusing on optimizing the term corresponding to the *total correlation*, a divergence $\text{KL}(q_\phi(\mathbf{z}) || \prod_d q_\phi(z_d))$; although the approaches differ, they share the common goal of aiming to induce interpretable, disentangled representations by minimizing this term, thus encouraging independence across the dimensions of \mathbf{z} .

As a further illustrative example, consider disentangling MNIST and Google Street-View House Numbers (SVHN)

images into constituent digit and “style”, an abstract variable which represents any aspects of the image not captured by the number itself. This is usually achieved by supervising the latent variable which corresponds to the digit and learning the style in an unsupervised manner [Kingma et al., 2014; Siddharth et al., 2017]. Alternatively, we could consider an unsupervised approach where we encode some one-hot encoded notion of digit as a set of dimensions of \mathbf{z} subject to a sparsity constraint; that is, a “digit” (or “identity”) is simply some representation for which only one entry is active at a time.

In this paper we reinterpret the standard VAE objective as a KL divergence between a generative model and its corresponding inference model. Doing so enables us to both synthesize various generalizations of the VAE objective and more clearly highlight the trade-offs associated with its optimization. Like recent approaches by Kim and Mnih [2018], Chen et al. [2018], Gao et al. [2018], we identify minimization of the total correlation as a means of inducing disentangled representations. We additionally derive a hierarchical decomposition of the the variational lower bound (named Hierarchically Factorized VAE or HFVAE) that enables use to induce different levels of statistical independence between groups of variables and between individual variables in the same group.

We evaluate our methodology on a variety of datasets including dSprites, MNIST, FMNIST and CelebA. Qualitative evaluation shows that our objective indeed uncovers interpretable features, whereas quantitative metrics demonstrate improvements over the state of the art. Moreover we show that the learned disentangled representations can recover combinations of features that were not present in the training set.

2 Background

Variational autoencoders (VAEs) jointly optimize two models. The generative model defines a distribution on a set of latent variables \mathbf{z} and observed data \mathbf{x} in terms of a prior $p(\mathbf{z})$ and a likelihood $p_\theta(\mathbf{x} | \mathbf{z})$, which is often referred to as the *decoder* model,

$$p_\theta(\mathbf{x}, \mathbf{z}) = p_\theta(\mathbf{x} | \mathbf{z})p(\mathbf{z}). \quad (1)$$

This distribution is estimated in tandem with an *encoder*, a conditional distribution $q_\phi(\mathbf{z} | \mathbf{x})$ which performs approximate inference in this model. This relationship between the generative model and the inference model motivate the “autoencoder” view of deep generative models.

If we denote the empirical data distribution as $q(\mathbf{x})$, then together with the encoder the inference model defines a

$$\begin{aligned}
\mathcal{L}(\theta, \phi) &= \mathbb{E}_{q_\phi(\mathbf{z}, \mathbf{x})} \left[\log \frac{p_\theta(\mathbf{x}, \mathbf{z})}{q_\phi(\mathbf{z}, \mathbf{x})} \right] = \mathbb{E}_{q_\phi(\mathbf{z}, \mathbf{x})} \left[\log \frac{p_\theta(\mathbf{x}, \mathbf{z})}{p_\theta(\mathbf{x})p(\mathbf{z})} + \log \frac{q_\phi(\mathbf{z})q(\mathbf{x})}{q_\phi(\mathbf{z}, \mathbf{x})} + \log \frac{p_\theta(\mathbf{x})}{q(\mathbf{x})} + \log \frac{p(\mathbf{z})}{q_\phi(\mathbf{z})} \right], \\
&= \mathbb{E}_{q_\phi(\mathbf{z}, \mathbf{x})} \left[\underbrace{\log \frac{p_\theta(\mathbf{x} | \mathbf{z})}{p_\theta(\mathbf{x})}}_{\textcircled{1}} - \underbrace{\log \frac{q_\phi(\mathbf{z} | \mathbf{x})}{q_\phi(\mathbf{z})}}_{\textcircled{2}} \right] - \underbrace{\text{KL}(q(\mathbf{x}) || p_\theta(\mathbf{x}))}_{\textcircled{3}} - \underbrace{\text{KL}(q_\phi(\mathbf{z}) || p(\mathbf{z}))}_{\textcircled{4}}.
\end{aligned}$$

Figure 2: *ELBO decomposition*. The VAE objective can be understood as minimizing the KL between a generative model $p_\theta(\mathbf{x}, \mathbf{z}) = p_\theta(\mathbf{x} | \mathbf{z})p(\mathbf{z})$ and an inference model $q_\phi(\mathbf{z}, \mathbf{x}) = q_\phi(\mathbf{z} | \mathbf{x})q(\mathbf{x})$. We can decompose this objective into 4 terms. Term $\textcircled{1}$, which can be intuitively thought of as the uniqueness of the reconstruction, is regularized by the mutual information $\textcircled{2}$, which represents the uniqueness of the encoding. Minimizing the KL in term $\textcircled{3}$ is equivalent to maximizing the marginal likelihood $\mathbb{E}_{q(\mathbf{x})}[\log p_\theta(\mathbf{x})]$. Combined maximization of $\textcircled{1} + \textcircled{3}$ is equivalent to maximizing $\mathbb{E}_{q_\phi(\mathbf{z}, \mathbf{x})}[\log p_\theta(\mathbf{x} | \mathbf{z})]$. Term $\textcircled{4}$ matches the inference marginal $q_\phi(\mathbf{z})$ to the prior $p(\mathbf{z})$, which in turn ensures realism for samples $\mathbf{x} \sim p_\theta(\mathbf{x})$ from the generative model.

joint distribution $q_\phi(\mathbf{z}, \mathbf{x})$, with

$$\begin{aligned}
q_\phi(\mathbf{z}, \mathbf{x}) &:= q_\phi(\mathbf{z} | \mathbf{x})q(\mathbf{x}), \\
q(\mathbf{x}) &:= \frac{1}{N} \sum_{n=1}^N \delta_{\mathbf{x}^n}(\mathbf{x}). \quad (2)
\end{aligned}$$

A VAE optimizes these two models using a single objective $\mathcal{L}(\theta, \phi)$, known as the evidence lower bound (ELBO),

$$\begin{aligned}
\mathcal{L}(\theta, \phi) &:= \frac{1}{N} \sum_{n=1}^N \mathbb{E}_{q_\phi(\mathbf{z} | \mathbf{x}^n)} \left[\log \frac{p_\theta(\mathbf{x}^n, \mathbf{z})}{q_\phi(\mathbf{z} | \mathbf{x}^n)} \right], \quad (3) \\
&= \mathbb{E}_{q(\mathbf{x})} \left[\log p_\theta(\mathbf{x}) - \text{KL}(q_\phi(\mathbf{z} | \mathbf{x}) || p_\theta(\mathbf{z} | \mathbf{x})) \right], \\
&\leq \mathbb{E}_{q(\mathbf{x})} [\log p_\theta(\mathbf{x})].
\end{aligned}$$

3 Objective Decomposition

A number of recent efforts have considered alternate decompositions of the VAE objective, both to formulate a better understanding of the trade-offs in optimizing VAE architectures and to identify generalizations that help induce desirable features such as disentangled representations. In order to summarize these efforts, we propose to express the VAE objective as a KL divergence

$$\begin{aligned}
\mathcal{L}(\theta, \phi) &:= -\text{KL}(q_\phi(\mathbf{z}, \mathbf{x}) || p_\theta(\mathbf{x}, \mathbf{z})), \quad (4) \\
&= \mathbb{E}_{q_\phi(\mathbf{z}, \mathbf{x})} \left[\frac{p_\theta(\mathbf{x}, \mathbf{z})}{q_\phi(\mathbf{z} | \mathbf{x})} \right] - \mathbb{E}_{q(\mathbf{x})} [\log q(\mathbf{x})].
\end{aligned}$$

This definition is equivalent to previous definitions since it only differs from the expression in Equation (3) by a constant, which is the entropy of the empirical data distribution $q(\mathbf{x})$.

$$H(\mathbf{x}) = -\mathbb{E}_{q(\mathbf{x})} [\log q(\mathbf{x})] = \log N. \quad (5)$$

An advantage of this interpretation as a KL divergence is that it becomes more apparent what it means to optimize the objective with respect to the generative model parameters θ and the inference model parameters ϕ (Figure 1). In particular, it is clear that the KL is minimized when $p_\theta(\mathbf{x}, \mathbf{z}) = q_\phi(\mathbf{z}, \mathbf{x})$, which in turn implies equality for the marginal $p_\theta(\mathbf{x}) = q(\mathbf{x})$. It also implies $q_\phi(\mathbf{z}) = p(\mathbf{z})$ for the marginal of the inference model,

$$q_\phi(\mathbf{z}) = \int q_\phi(\mathbf{z}, \mathbf{x}) d\mathbf{x} = \frac{1}{N} \sum_{n=1}^N q_\phi(\mathbf{z} | \mathbf{x}^n). \quad (6)$$

To better understand the trade-offs involved in optimizing the VAE objective, we can perform a decomposition (Figure 2) similar to the one obtained by Hoffman and Johnson [2016]. This decomposition contains 4 terms. Terms $\textcircled{3}$ and $\textcircled{4}$ enforce consistency between the marginal distributions over \mathbf{x} and \mathbf{z} . Minimizing the KL in term $\textcircled{3}$ maximizes the marginal likelihood $\mathbb{E}_{q(\mathbf{x})}[\log p_\theta(\mathbf{x})]$, whereas minimizing $\textcircled{4}$ ensures that the inference marginal $q_\phi(\mathbf{z})$ approximates the prior $p(\mathbf{z})$.

Terms $\textcircled{1}$ and $\textcircled{2}$ enforce consistency between the conditional distributions. Intuitively speaking, term $\textcircled{1}$ maximizes the identifiability of the values \mathbf{z} that generate each \mathbf{x}^n ; when we sample $\mathbf{z} \sim q_\phi(\mathbf{z} | \mathbf{x}^n)$, then the likelihood $p_\theta(\mathbf{x}^n | \mathbf{z})$ under the generative model should be *higher* than the marginal likelihood $p_\theta(\mathbf{x}^n)$. Term $\textcircled{2}$ regularizes term $\textcircled{1}$ by minimizing the mutual information $I(\mathbf{z}; \mathbf{x})$ between \mathbf{x} and \mathbf{z} in the inference model, which means that $q_\phi(\mathbf{z} | \mathbf{x}^n)$ maps each \mathbf{x}^n to less identifiable values.

Note that evaluation of term $\textcircled{1}$ is intractable in practice, since we are not able to pointwise evaluate $p_\theta(\mathbf{x})$. We can circumvent this intractability by combining $\textcircled{1} + \textcircled{3}$

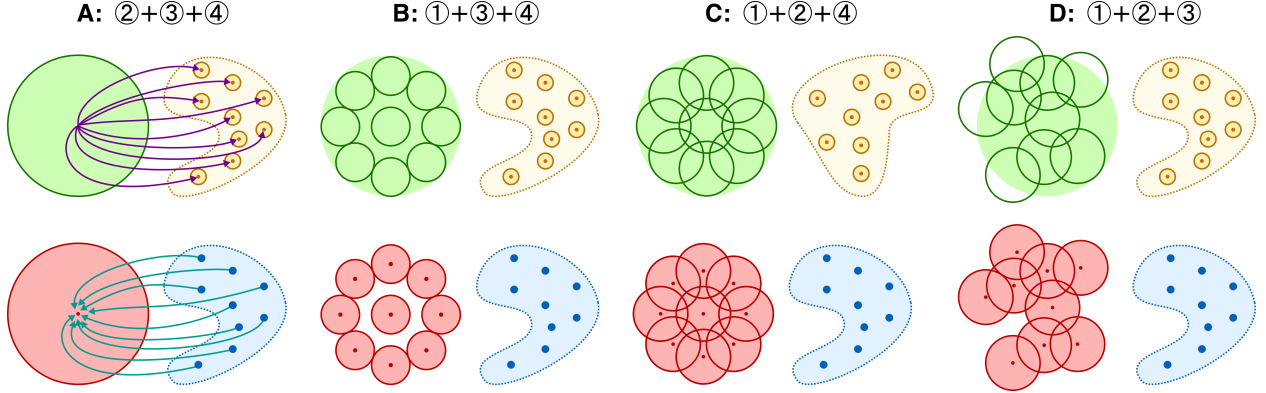


Figure 3: Illustration of the role of each of the term in the decomposition from Figure 2. Each figure shows the effect of removing one term from the objective. **A:** Removing ① means that we no longer require a unique \mathbf{z} for each \mathbf{x}^n . Term ② will then minimize $I(\mathbf{x}; \mathbf{z})$ which means that each \mathbf{x}^n is mapped to the prior. **B:** Removing ② eliminates the constraint that $I(\mathbf{x}; \mathbf{z})$ must be small under the inference model, causing each \mathbf{x}^n to be mapped to a smaller region in \mathbf{z} space. **C:** Removing ③ eliminates the constraint that $p_\theta(\mathbf{x})$ must match $q(\mathbf{x})$. **D:** Removing ④ eliminates the constraint that $q_\phi(\mathbf{z})$ must match $p(\mathbf{z})$.

into a single term, which recovers the reconstruction error

$$\begin{aligned} \operatorname{argmax}_{\theta, \phi} \mathbb{E}_{q_\phi(\mathbf{z}, \mathbf{x})} \left[\log \frac{p_\theta(\mathbf{x} | \mathbf{z})}{p_\theta(\mathbf{x})} + \log \frac{p_\theta(\mathbf{x})}{q(\mathbf{x})} \right] \\ = \operatorname{argmax}_{\theta, \phi} \mathbb{E}_{q_\phi(\mathbf{z}, \mathbf{x})} [\log p_\theta(\mathbf{x} | \mathbf{z})]. \end{aligned}$$

Given that the terms ②, ③ and ④ are bounded from above by 0, we can interpret the decomposition in Figure 2 as a Lagrangian relaxation of the constrained optimization problem (see, e.g., Alemi et al. [2016])

$$\begin{aligned} \max_{\theta, \phi} \quad & \mathbb{E}_{q_\phi(\mathbf{x}, \mathbf{z})} \left[\log \frac{p_\theta(\mathbf{x} | \mathbf{z})}{p_\theta(\mathbf{x})} \right], & \text{①} \\ \text{s.t.} \quad & I(\mathbf{x}; \mathbf{z}) = 0, & \text{②} \\ & \text{KL}(q(\mathbf{x}) || p_\theta(\mathbf{x})) = 0, & \text{③} \\ & \text{KL}(q_\phi(\mathbf{z}) || p(\mathbf{z})) = 0. & \text{④} \end{aligned}$$

for which we can define the Lagrangian

$$\mathcal{L}(\theta, \phi) = \text{①} - \lambda_2 \text{②} - \lambda_3 \text{③} - \lambda_4 \text{④}. \quad (7)$$

We can now adjust each of the Lagrange multipliers $\lambda_2, \lambda_3, \lambda_4$ in order to control which of our constraints we are willing to relax more, and which of our constraints we would like to relax less. To build intuition for what it means to relax each of these constraints, Figure 3 shows the effect of removing each term from the objective. When we remove ③ or ④ we can learn models in which $p_\theta(\mathbf{x})$ deviates from $q(\mathbf{x})$ or $p_\phi(\mathbf{z})$ deviates from $p(\mathbf{z})$. When we remove ① we remove the requirement that $p_\theta(\mathbf{x}^n | \mathbf{z})$ should be higher when $\mathbf{z} \sim q_\phi(\mathbf{z} | \mathbf{x}^n)$ than when $\mathbf{z} \sim p(\mathbf{z})$. Provided the decoder model is sufficiently expressive, we will then learn a generative model

that ignores the latent code \mathbf{z} . This type of solution does in fact arise in certain cases, even when ① is included in the objective, particularly when using auto-regressive decoder architectures [Chen et al., 2016].

When we remove ②, we learn a model that minimizes overlap between encoder distributions $q_\phi(\mathbf{z} | \mathbf{x}^n)$ when conditioned on different data points \mathbf{x}^n in order to maximize ①. This maximizes the mutual information $I(\mathbf{x}; \mathbf{z})$, which is bounded from above by $\log N$. In practice ② often saturates to $\log N$, even when included in the objective, which suggests that maximizing ① outweighs this cost, at least for the encoder/decoder architectures that are commonly considered in present-day models.

4 Hierarchically Factorized VAEs

In the context of this paper, we are interested in using the decomposition from Figure 2 to define an objective that will induce disentangled representations by encouraging statistical independence between features. The β -VAE objective [Higgins et al., 2016] aims to achieve this goal by defining the Lagrangian relaxation

$$\begin{aligned} \mathcal{L}^{\beta\text{-VAE}}(\theta, \phi) = \mathbb{E}_{q(\mathbf{x})} \left[\mathbb{E}_{q_\phi(\mathbf{z} | \mathbf{x})} [\log p_\theta(\mathbf{x} | \mathbf{z})] \right. \\ \left. - \beta \text{KL}(q_\phi(\mathbf{z} | \mathbf{x}) || p(\mathbf{z})) \right]. \end{aligned}$$

We can express this objective in the terms of Figure 2 as

$$\mathcal{L}^{\beta\text{-VAE}}(\theta, \phi) = \text{①} + \text{③} + \beta \left(\text{②} + \text{④} \right).$$

In order to induce disentangled representations, the authors set $\beta > 1$. This works well in certain cases, but

$$\begin{aligned}
-\text{KL}(q_\phi(\mathbf{z}) \parallel p(\mathbf{z})) &= -\mathbb{E}_{q_\phi(\mathbf{z})} \left[\log \frac{q_\phi(\mathbf{z})}{p(\mathbf{z})} \right] = -\mathbb{E}_{q_\phi(\mathbf{z})} \left[\log \frac{q_\phi(\mathbf{z})}{\prod_d q_\phi(\mathbf{z}_d)} + \log \frac{\prod_d q_\phi(\mathbf{z}_d)}{\prod_d p(\mathbf{z}_d)} + \log \frac{\prod_d p(\mathbf{z}_d)}{p(\mathbf{z})} \right] \\
&= \underbrace{\mathbb{E}_{q_\phi(\mathbf{z})} \left[\log \frac{p(\mathbf{z})}{\prod_d p(\mathbf{z}_d)} - \log \frac{q_\phi(\mathbf{z})}{\prod_d q_\phi(\mathbf{z}_d)} \right]}_{\textcircled{A}} - \underbrace{\sum_d \text{KL}(q_\phi(\mathbf{z}_d) \parallel p(\mathbf{z}_d))}_{\textcircled{B}}. \\
-\text{KL}(q_\phi(\mathbf{z}_{d,e}) \parallel p(\mathbf{z}_{d,e})) &= \mathbb{E}_{q_\phi(\mathbf{z}_d)} \left[\underbrace{\log \frac{p(\mathbf{z}_d)}{\prod_e p(\mathbf{z}_{d,e})}}_{\textcircled{i}} - \underbrace{\log \frac{q_\phi(\mathbf{z}_d)}{\prod_e q_\phi(\mathbf{z}_{d,e})}}_{\textcircled{ii}} \right] - \sum_e \text{KL}(q_\phi(\mathbf{z}_{d,e}) \parallel p(\mathbf{z}_{d,e}))
\end{aligned}$$

Figure 4: *Hierarchical KL decomposition*. We can decompose term $\textcircled{4}$ into subcomponents \textcircled{A} and \textcircled{B} . Term \textcircled{A} matches the total correlation between variables in the inference model relative to the total correlation under the generative model. Term \textcircled{B} minimizes the KL divergence between the inference marginal and prior marginal for each variable \mathbf{z}_d . When the variables \mathbf{z}_d contain sub-variables $\mathbf{z}_{d,e}$, we can recursively decompose the KL on the marginals \mathbf{z}_d into term \textcircled{i} , which matches the total correlation \textcircled{ii} . Thus, it minimizes per-dimension KL divergence.

it has the drawback in that it also increases the strength of $\textcircled{2}$, which means that the encoder model may discard more information about \mathbf{x} in order to minimize the mutual information $I(\mathbf{x}; \mathbf{z})$.

4.1 KL decomposition

Looking at the β -VAE objective, it seems intuitive that increasing the weight of term $\textcircled{4}$ is likely to aid disentanglement. One notion of disentanglement is that there should be a low degree of correlation between different latent variables \mathbf{z}_d . If we choose the a prior $p(\mathbf{z}) = \prod_d p(\mathbf{z}_d)$ in which different variables are independent, then minimizing the KL term should induce an inference marginal $q_\phi(\mathbf{z}) = \prod_d q_\phi(\mathbf{z}_d)$ in which \mathbf{z}_d are also independent.

As also noted by Kim and Mnih [2018] and Chen et al. [2018], we can introduce an additional level of decomposition for $\textcircled{4}$ in the objective (Figure 4). As with term $\textcircled{1} + \textcircled{2}$, the term \textcircled{A} consists of two components. The second of these terms minimizes the total correlation (TC), which is a generalization of the mutual information to more than two variables,

$$\begin{aligned}
TC(\mathbf{z}) &= E_{q_\phi(\mathbf{z})} \left[\log \frac{q_\phi(\mathbf{z})}{\prod_d q_\phi(\mathbf{z}_d)} \right], \\
&= \text{KL} \left(q_\phi(\mathbf{z}) \parallel \prod_d q_\phi(\mathbf{z}_d) \right). \tag{8}
\end{aligned}$$

Minimizing the total correlation means that we will learn $q_\phi(\mathbf{z})$ in which different \mathbf{z}_d are statistically independent, thereby inducing disentanglement.

The first component of \textcircled{A} is not present in the objectives defined by Kim and Mnih [2018] and Chen et al. [2018]. It

maximizes the probability of $p(\mathbf{z})$ under the prior, relative to the probability of the product of marginals $\prod_d p(\mathbf{z}_d)$. Note that this form is analogous to $\textcircled{1}$, which maximizes $p_\theta(\mathbf{x}, \mathbf{z})$ relative to the product of marginals $p_\theta(\mathbf{x})p(\mathbf{z})$. Maximizing \textcircled{A} with respect to ϕ will match the total correlation in $q(\mathbf{z})$ to the total correlation in $p(\mathbf{z})$. When $p(\mathbf{z}) = \prod_d p(\mathbf{z}_d)$ we recover the term from Kim and Mnih [2018] and Chen et al. [2018].

In cases where \mathbf{z}_d itself represents a group of variables, rather than a single variable, we can now continue to decompose to another set of terms \textcircled{i} and \textcircled{ii} which match the total correlation for \mathbf{z}_d and the KL divergences for constituent variables $\mathbf{z}_{d,e}$. We could in principle continue this decomposition for any number of levels. This provides an opportunity to induce hierarchies of disentangled features. For example, when modeling MNIST we may wish to emphasize the constraint that the digit identity (which is a discrete variable) should be uncorrelated with variables that characterize the handwriting style. That said for other variables it is less obvious that there should be no correlations. For example, there could be a causal relationship between the pen stroke width and the size of openings. In this case we may want to impose a higher level of regularization on the correlation between digit identity and style variables than on the correlation between style variables themselves.

4.2 Approximation of the Objective

In order to induce hierarchically factored representations we will employ an objective of the form

$$\begin{aligned}
\mathcal{L}(\theta, \phi) &= \textcircled{1} + \textcircled{3} + \textcircled{ii} \\
&+ \alpha \textcircled{2} + \beta \textcircled{A} + \gamma \textcircled{i}. \tag{9}
\end{aligned}$$

Paper	Objective
Kingma and Welling [2013] Rezende et al. [2014]	① + ② + ③ + ④
Higgins et al. [2016]	① + ③ + β (② + ④)
Kumar et al. [2017]	① + ② + ③ + λ ④
Zhao et al. [2017]	① + ③ + λ ④
Gao et al. [2018]	① + ② + ③ + ④ - λ ② ^a
Achille and Soatto [2018]	① + ③ + β ② + γ ④*
Kim and Mnih [2018] Chen et al. [2018]	① + ② + ③ + ⑥ + β ④*
HFVAE (this paper)	① + ③ + ② + α ② + β ④ + γ ①

Table 1: Comparison of objectives in autoencoding deep generative models. The objective in this paper is most closely related to recent work by Kim and Mnih [2018] and Chen et al. [2018], but incorporates an additional level of hierarchical decomposition. The asterisk (A)* indicates that the prior factorizes, i.e. $p(\mathbf{z}) = \prod_d p(\mathbf{z}_d)$. The notation (2)^a refers to restriction of the mutual information (2) to a subset of "Anchor" variables \mathbf{z}_a .

In this objective α controls the amount of $I(\mathbf{x}; \mathbf{z})$ regularization. We include it for completeness, although we find in practice that $I(\mathbf{x}; \mathbf{z})$ saturates in the cases that we consider in our experimental evaluation. The term β controls the TC regularization between groups of variables, whereas γ controls the TC regularization for individual variables.

In order to optimize this objective, we need to approximate the inference marginals $q_\phi(\mathbf{z})$, $q_\phi(\mathbf{z}_d)$, and $q_\phi(\mathbf{z}_{d,e})$. Computing these quantities exactly requires a full pass over the dataset, since $q_\phi(\mathbf{z})$ is a mixture over all data points in the training set

$$q_\phi(\mathbf{z}) = \frac{1}{N} \sum_{n=1}^N q_\phi(\mathbf{z} | \mathbf{x}^n). \quad (10)$$

We approximate $q_\phi(\mathbf{z})$ with a Monte Carlo estimate of $\hat{q}_\phi(\mathbf{z})$ over the same batch of samples that we use to approximate all other terms in the objective $\mathcal{L}(\theta, \phi)$. For simplicity we will consider the term

$$\mathbb{E}_{q_\phi(\mathbf{z}, \mathbf{x})}[\log q_\phi(\mathbf{z})] \simeq \frac{1}{B} \sum_{b=1}^B \log q_\phi(\mathbf{z}^{(b)}), \quad (11)$$

where $\mathbf{z}^{(b)}$ is sampled via the normal construction by selecting a batch of items $\mathbf{x}^{(b)}$ and then sampling from the inference model

$$\begin{aligned} \mathbf{x}^{(b)} &\sim q(\mathbf{x}), \\ \mathbf{z}^{(b)} &\sim q_\phi(\mathbf{z} | \mathbf{x}^{(b)}). \end{aligned} \quad (12)$$

We define the estimate of $\hat{q}_\phi(\mathbf{z}^{(b)})$ as (see Appendix A.1)

$$\begin{aligned} \hat{q}_\phi(\mathbf{z}^{(b)}) &= \frac{1}{N} q_\phi(\mathbf{z}^{(b)} | \mathbf{x}^{(b)}) \\ &+ \frac{N-1}{N(B-1)} \sum_{b' \neq b} q_\phi(\mathbf{z}^{(b)} | \mathbf{x}^{(b')}). \end{aligned} \quad (13)$$

We can think of this approximation as a partially stratified sample, in which we deterministically include the term $\mathbf{x}^n = \mathbf{x}^{(b)}$ and compute a Monte Carlo estimate over the remaining terms, treating samples $\mathbf{x}^{(b')}$ for $b' \neq b$ as samples from the distribution $q(\mathbf{x} | \mathbf{x} \neq \mathbf{x}^{(b)})$.

We now substitute $\log \hat{q}_\phi(\mathbf{z})$ for $\log q_\phi(\mathbf{z})$ in Equation (11). By Jensen's inequality this yields a lower bound on our original expectation since

$$\mathbb{E} \left[\frac{1}{B} \sum_{b=1}^B \log \hat{q}_\phi(\mathbf{z}^{(b)}) \right] \leq \frac{1}{B} \sum_{b=1}^B \log \mathbb{E} \left[\hat{q}_\phi(\mathbf{z}^{(b)}) \right].$$

The fact that our approximation is a *lower* bound means that minimizing (ii) is equivalent to maximizing an *upper* bound (note that is (2) = $-\text{KL}(q_\phi(\mathbf{z}) || p(\mathbf{z}))$). That said, the estimator is consistent, which means that in practice the bias is likely sufficient small given the batch sizes that are needed to approximate the inference marginal (512-1024).

5 Related Work

This work is closely related to a number of recently proposed generalizations of VAE objectives, which we summarize in Table 1. As noted above, the β -VAE objective [Higgins et al., 2016] uses a multiplier $\beta > 1$ for the terms (2) and (4). In settings where we are not primarily interested in inducing disentangled representations, β -VAE objective has also been used with $\beta < 1$ in order to *increase* the quality of reconstructions (see, e.g., [Alemi et al., 2016; Engel et al., 2017; Liang et al., 2018]). This also decreases the relative weight of (2), but this in practice does not influence the learned representation in cases where $I(\mathbf{x}; \mathbf{z})$ saturates anyway.

Zhao et al. [2017] consider an objective that eliminates the mutual information (2) entirely and assigns an additional weight to the KL divergence between $q_\phi(\mathbf{z})$ and $p(\mathbf{z})$ in (4). Kumar et al. [2017] approximates the KL divergence in (4) by matching the covariance of $q_\phi(\mathbf{z})$ and

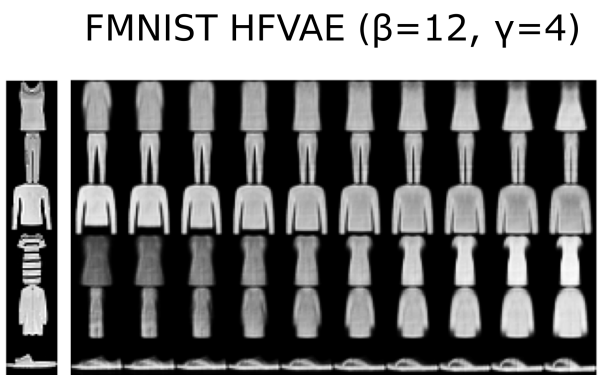


Figure 5: MNIST and FMNIST reconstructions for z_d values ranging from -3 to 3. Rows contain both different samples from the dataset and different dimensions d .

$p(z)$. Recent work by Gao et al. [2018] connects VAEs to the principle of correlation explanation, and defines an objective that reduces the mutual information regularization in ② for a subset of "Anchor" variables z_a . Achille and Soatto [2018] approach VAEs from an information bottleneck perspective and introduce a TC term into the objective.

The KL decomposition in Figure 4 is very similar to the one that was recently introduced by Kim and Mnih [2018] and Chen et al. [2018]. It induce disentangled representations by increasing the weight of ① to minimize the total correlation. Relative to these approaches two we here take a slightly more general perspective:

1. We impose a hierarchical structure on our model by identifying groups of variables z_d , which allows us to control the weight of ① relative to the weight of term ② to ensure that the total correlation between groups of variables is enforced more rigorously than the total correlation within groups of variables.

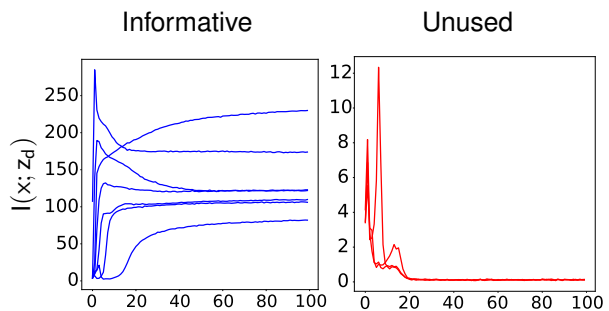


Figure 6: The HFVAE objective prunes unnecessary features. Shown is the mutual information ② for each individual dimension $I(x; z_d)$. For uninformative dimensions (right) the mutual information decreases to 0.

Model	FactorVAE	Eastwood
VAE	0.71	0.40
β -VAE ($\beta = 4.0$)	0.72	0.71
β -SVAE ($\beta = 4.0$)	0.47	0.19
β -TCVAE ($\beta = 4.0$)	0.71	0.31
HFVAE ($\beta = 4.0, \gamma = 3.0$)	0.78	0.74

Table 2: Disentanglement scores for the dSprites dataset [Higgins et al., 2016] using the metrics proposed by Kim and Mnih [2018] and Eastwood and Williams [2018].

2. Rather than a diagonal Gaussian prior $p(z)$, we consider priors that combine discrete and continuous variables and can incorporate parameters $p_\theta(z)$ to learn a covariance structure (for continuous variables) or conditional probabilities (for discrete variables).

6 Experiments

In order to assess how the HFVAE objective performs relative to existing approaches, we evaluate a variety of datasets and tasks. We consider 4 datasets:

dSprites [Higgins et al., 2016]: 737,280 binary 64×64 images of 2D shapes with ground truth factors.

MNIST [LeCun et al., 2010]: 60000 gray-scale 32×32 images of handwritten digits.

Fashion-MNIST [Xiao et al., 2017]: 60000 gray-scale 32×32 images of clothing items divided in 10 classes.

CelebA [Liu et al., 2015]: 202,599 RGB $64 \times 64 \times 3$ images of celebrity faces.

On these datasets we compare a number of objectives and priors. The objectives we compare are the standard VAE objective [Kingma and Welling, 2013; Rezende et al., 2014], the β -VAE objective [Higgins et al., 2016], the

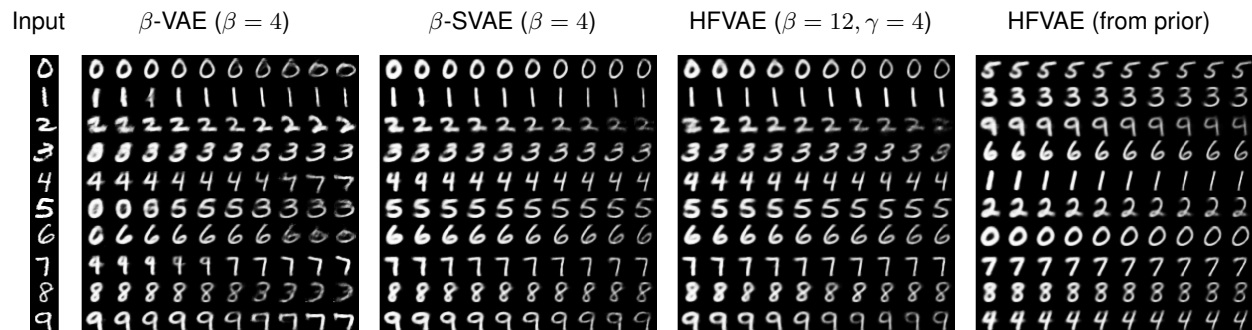


Figure 7: Manipulation of the thickness variable of the range -3 to 3. The β -VAE is not able to maintain digit identity as we vary thickness. The SVAE and HFVAE, which incorporate a discrete variable into the prior, are able to maintain the digit identity across the entire range.

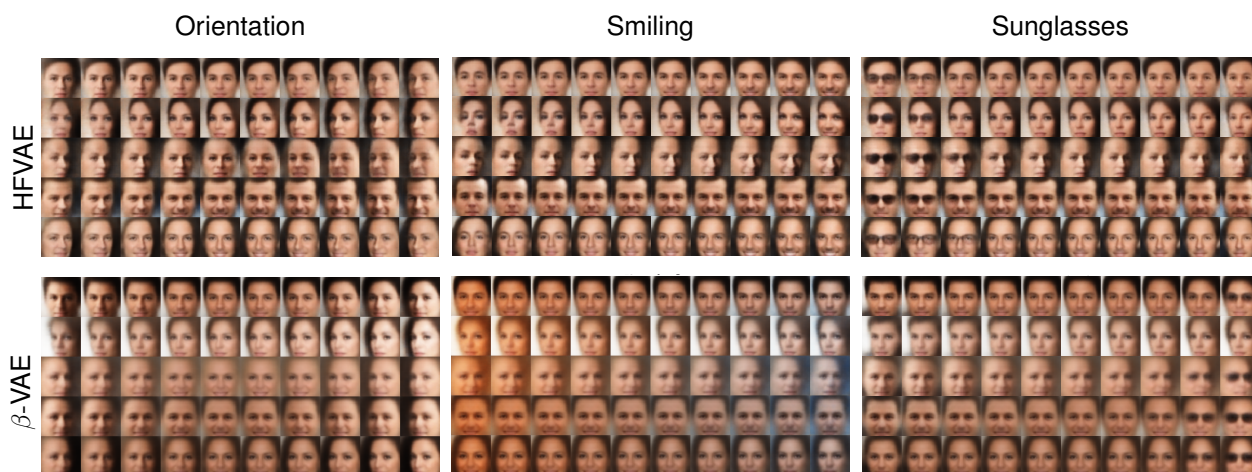


Figure 8: Interpretable factors in CelebA for a HFVAE ($\beta = 5.0, \gamma = 3.0$) and a β -VAE ($\beta = 8.0$)

TC-VAE objective [Chen et al., 2018], and our HFVAE objective. The priors $p(\mathbf{z})$ that we employ are:

VAE, β -VAE, TCVAE: A diagonal Gaussian prior with 10 dimensions (*dSprites*, *MNIST*, *FMNIST*), or 20 dimensions (*CelebA*).

β -SVAE, HFVAE: A mixed Gaussian discrete prior. *MNIST*, *FMNIST*: 1 10-dimensional Gaussian variable, 1 discrete variable with 10 classes. *dSprites*: 1 10-dimensional Gaussian variable, 1 discrete variable with 3 classes. *CelebA*: 1 20-dimensional Gaussian variable, 2 Bernoulli variables.

We train using Adam with default parameters using batch sizes between 512 and 1024. Model architectures are described in Appendix B.

6.1 Interpretability of Features

We begin with a qualitative evaluation of the features that are identified when training with the HFVAE objective. Figure 5 shows results for the MNIST data and the FMNIST data. For the MNIST data the representation recovers 7 interpretable features. For the remaining 3 features the mutual information term $I(\mathbf{x}; \mathbf{z}_d)$ decreases to 0 as can be seen in Figure 6. Similarly for the CelebA dataset (see Figure 8) we uncover interpretable features such as the orientation of the face, variation from smiling to non-smiling, and the presence of sunglasses.

6.2 Quantitative Metrics on dSprites

As a quantitative assessment of the quality of learned representations, we evaluate the metrics proposed by Kim and Mnih [2018] and Eastwood and Williams [2018]. For the Eastwood and Williams metric, we used a random forest as the regressor from features and ground-truth

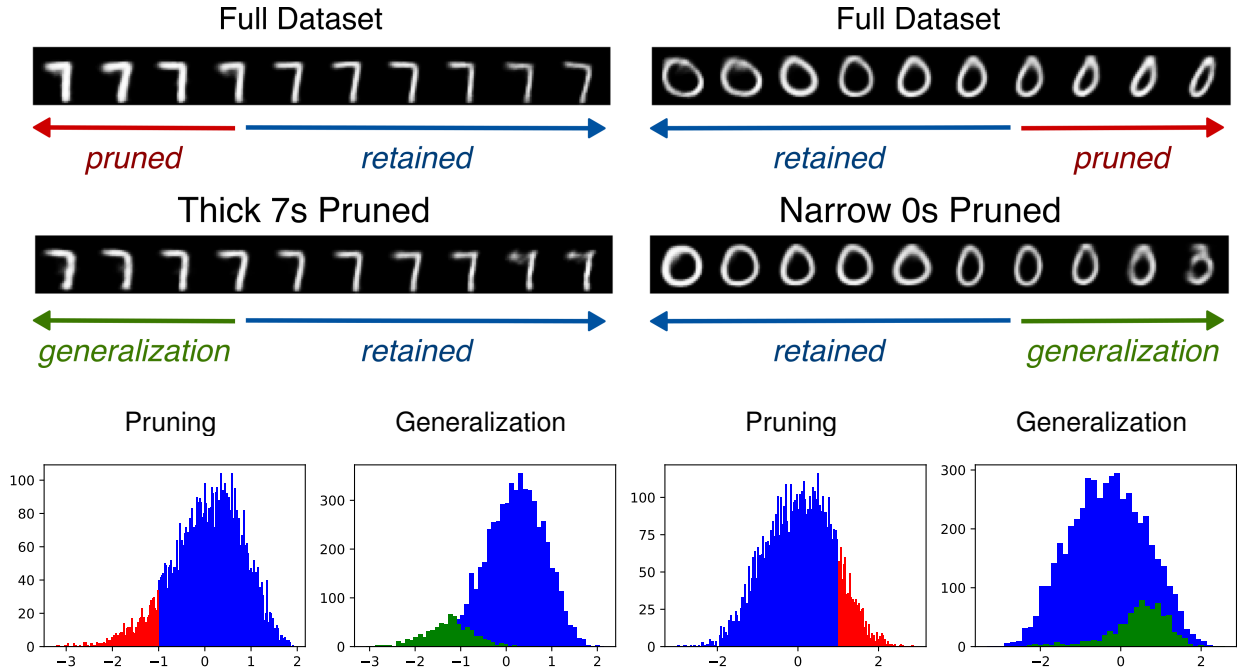


Figure 9: Generalization to unseen combinations of factors. A HFVAE is trained on the full dataset, after a subset of the data is pruned. We then test generalization of a model trained on the pruned dataset to the removed portion of the data.

factors. In Table 1, we list these metrics for each of the model types and objectives defined above. The HFVAE outperforms other approaches.

6.3 Unsupervised Learning of Discrete Labels

The ability of the model to disentangle discrete variables depends on how separable the classes of objects are for a given dataset. In the case of the Fashion-MNIST, the classes (i.e. the clothing items) are distinctive enough that our model can capture it in the discrete variable. On the other hand, in the case of the dSprites dataset, the shapes are very similar, which makes it difficult for our model to capture them effectively in a discrete variable. The MNIST dataset resides in the middle of this spectrum (For example, it is possible to convert a 9 into a 4 under some continuous variation).

In figure 7, we have sampled one data point for each digit and vary its thickness variable for each of the models - β -VAE, β -structured VAE, and HFVAE. Clearly, a structured VAE does a better job at disentangling digit vs thickness. The major advantage of HFVAE compared to β -structured VAE is the ability to generate samples from the prior which captures the digit. We found that β -structured VAE failed to disentangle the digit from style, and the samples generated from the discrete prior does not corresponds to a distinct digit.

6.4 Zero-shot Generalization

One of the desiderata of disentangled representations is that they should not only capture distinct interpretable factors of variation, but also allow generalization to previously unseen combinations of features. For example, we can imagine a pink elephant even when we have not encountered such an object before.

To test whether our learned representations exhibit these generalization properties, we perform the following experiment. We first train the HFVAE on the MNIST dataset. We then prune some fraction of the data. We will here consider the case where we prune 7s with a high stroke thickness and 0s with a narrow character width. We then train a new HFVAE model on the the pruned dataset and use the removed portion of the data as a test set to evaluate generalization properties.

Figure 9 shows the results of this experiment. As we can see, the model trained on pruned data is able to reconstruct digits with values for the stroke and character width that were never seen during training. The histograms for the feature values show that the encoder model is similarly able to extract features from previously unseen examples.

7 Discussion

Much of the work on learning disentangled representations thus far has focused on cases where the distinct

factors of variation take the form of a set of scalar variables that are uncorrelated and for which supervision could in principle be obtained. As we begin to apply these techniques to real world datasets we are likely to encounter many forms of correlations between latent variables, particularly when there are causal dependencies between these variables. This work presents a first step in the direction of enabling the learning of more structured disentangled representations. By enforcing statistical independence between groups of variables, we are now, in principle able to disentangle variables that have higher-dimensional representations. An avenue of future work is to develop datasets that allow us to more rigorously test our ability to extract such higher-dimensional variables.

References

- A. Achille and S. Soatto. Information Dropout: Learning Optimal Representations Through Noisy Computation. *IEEE Transactions on Pattern Analysis and Machine Intelligence*, PP(99):1–1, 2018.
- Alexander A. Alemi, Ian Fischer, Joshua V. Dillon, and Kevin Murphy. Deep Variational Information Bottleneck. *arXiv:1612.00410 [cs, math]*, December 2016.
- Diane Bouchacourt, Ryota Tomioka, and Sebastian Nowozin. Multi-level variational autoencoder: Learning disentangled representations from grouped observations. *arXiv preprint arXiv:1705.08841*, 2017.
- Samuel R Bowman, Luke Vilnis, Oriol Vinyals, Andrew M Dai, Rafal Jozefowicz, and Samy Bengio. Generating sentences from a continuous space. *CoNLL 2016*, page 10, 2016.
- Tian Qi Chen, Xuechen Li, Roger Grosse, and David Duvenaud. Isolating sources of disentanglement in variational autoencoders. *arXiv preprint arXiv:1802.04942*, 2018.
- Xi Chen, Diederik P. Kingma, Tim Salimans, Yan Duan, Prafulla Dhariwal, John Schulman, Ilya Sutskever, and Pieter Abbeel. Variational lossy autoencoder. *arXiv preprint arXiv:1611.02731*, 2016.
- Cian Eastwood and Christopher K. I. Williams. A Framework for the Quantitative Evaluation of Disentangled Representations. In *International Conference on Learning Representations*, February 2018.
- Jesse Engel, Matthew Hoffman, and Adam Roberts. Latent Constraints: Learning to Generate Conditionally from Unconditional Generative Models. *arXiv:1711.05772 [cs, stat]*, November 2017.
- Shuyang Gao, Rob Breckelmanns, Greg Ver Steeg, and Aram Galstyan. Auto-encoding total correlation explanation. *arXiv preprint arXiv:1802.05822*, 2018.
- Leon A Gatys, Alexander S Ecker, and Matthias Bethge. A neural algorithm of artistic style. *arXiv preprint arXiv:1508.06576*, 2015.
- Rafael Gómez-Bombarelli, Jennifer N Wei, David Duvenaud, José Miguel Hernández-Lobato, Benjamín Sánchez-Lengeling, Dennis Sheberla, Jorge Aguilera-Iparraguirre, Timothy D Hirzel, Ryan P Adams, and Alán Aspuru-Guzik. Automatic chemical design using a data-driven continuous representation of molecules. *ACS Central Science*, 2018.
- Ishaan Gulrajani, Kundan Kumar, Faruk Ahmed, Adrien Ali Taiga, Francesco Visin, David Vazquez, and Aaron Courville. PixelVAE: A latent variable model for natural images. In *International Conference on Machine Learning*, 2017.
- Irina Higgins, Loic Matthey, Arka Pal, Christopher Burgess, Xavier Glorot, Matthew Botvinick, Shakir Mohamed, and Alexander Lerchner. beta-VAE: Learning basic visual concepts with a constrained variational framework. In *International Conference on Learning Representations*, 2016.
- Matthew D. Hoffman and Matthew J. Johnson. Elbo surgery: Yet another way to carve up the variational evidence lower bound. In *Workshop in Advances in Approximate Bayesian Inference, NIPS*, 2016.
- Matthew Johnson, David K Duvenaud, Alex Wiltschko, Ryan P Adams, and Sandeep R Datta. Composing graphical models with neural networks for structured representations and fast inference. In *Advances in Neural Information Processing Systems*, pages 2946–2954, 2016.
- Hyunjik Kim and Andriy Mnih. Disentangling by factorising. *arXiv preprint arXiv:1802.05983*, 2018.
- Diederik P. Kingma and Max Welling. Auto-encoding variational bayes. In *International Conference on Learning Representations*, 2013.
- Diederik P Kingma, Shakir Mohamed, Danilo Jimenez Rezende, and Max Welling. Semi-supervised learning with deep generative models. In *Advances in Neural Information Processing Systems*, pages 3581–3589, 2014.
- Tejas D Kulkarni, William F Whitney, Pushmeet Kohli, and Josh Tenenbaum. Deep convolutional inverse graphics network. In *Advances in Neural Information Processing Systems*, pages 2539–2547, 2015.
- Abhishek Kumar, Prasanna Sattigeri, and Avinash Balakrishnan. Variational inference of disentangled latent concepts from unlabeled observations. *arXiv preprint arXiv:1711.00848*, 2017.
- Matt J Kusner, Brooks Paige, and José Miguel Hernández-Lobato. Grammar variational autoencoder. In *International Conference on Machine Learning*, 2017.
- Yann LeCun, Corinna Cortes, and CJ Burges. Mnist handwritten digit database. *AT&T Labs [Online]*. Available: <http://yann.lecun.com/exdb/mnist>, 2, 2010.
- Dawen Liang, Rahul G. Krishnan, Matthew D. Hoffman, and Tony Jebara. Variational Autoencoders for Collaborative Filtering. *arXiv:1802.05814 [cs, stat]*, February 2018.
- Ziwei Liu, Ping Luo, Xiaogang Wang, and Xiaoou Tang. Deep learning face attributes in the wild. In *Proceedings of the IEEE International Conference on Computer Vision*, pages 3730–3738, 2015.
- Aaron van den Oord, Sander Dieleman, Heiga Zen, Karen Simonyan, Oriol Vinyals, Alex Graves, Nal Kalchbrenner, Andrew Senior, and Koray Kavukcuoglu. Wavenet: A generative model for raw audio. *arXiv preprint arXiv:1609.03499*, 2016.
- Daniilo Jimenez Rezende, Shakir Mohamed, and Daan Wierstra. Stochastic backpropagation and approximate inference in deep generative models. In *Proceedings of The 31st International Conference on Machine Learning*, pages 1278–1286, 2014.
- N Siddharth, Brooks Paige, Jan-Willem Van de Meent, Alban Desmaison, Frank Wood, Noah D Goodman, Pushmeet Kohli,

- and Philip HS Torr. Learning disentangled representations with semi-supervised deep generative models. In *Advances in Neural Information Processing Systems*, 2017.
- Lucas Theis, Wenzhe Shi, Andrew Cunningham, and Ferenc Huszár. Lossy image compression with compressive autoencoders. *arXiv preprint arXiv:1703.00395*, 2017.
- Han Xiao, Kashif Rasul, and Roland Vollgraf. Fashion-mnist: a novel image dataset for benchmarking machine learning algorithms, 2017.
- Weidi Xu, Haoze Sun, Chao Deng, and Ying Tan. Variational autoencoder for semi-supervised text classification. In *AAAI*, pages 3358–3364, 2017.
- Shengjia Zhao, Jiaming Song, and Stefano Ermon. InfoVAE: Information maximizing variational autoencoders. *arXiv preprint arXiv:1706.02262*, 2017.

A Appendix

A.1 Approximating the Inference Marginal

We will here derive a Monte Carlo estimator for the entropy of the marginal $q_\phi(\mathbf{z})$ of the inference model

$$H_\phi[\mathbf{z}] = -\mathbb{E}_{q_\phi(\mathbf{z})} [\log q_\phi(\mathbf{z})]. \quad (14)$$

As with other terms in the objective, we can approximate this expectation by sampling $\mathbf{z}^{(b)} \sim q_\phi(\mathbf{z})$ using,

$$\mathbf{x}^{(b)} \sim q(\mathbf{x}), \quad b = 1, \dots, B, \quad (15)$$

$$\mathbf{z}^{(b)} \sim q_\phi(\mathbf{z} \mid \mathbf{x}^{(b)}). \quad (16)$$

We now additionally need to approximate the values,

$$\log q_\phi(\mathbf{z}^{(b)}) = \log \left[\frac{1}{N} \sum_{n=1}^N q_\phi(\mathbf{z}^{(b)} \mid \mathbf{x}^n) \right]. \quad (17)$$

We will do so by pulling the term for which $\mathbf{x}^n = \mathbf{x}^{(b)}$ out of the sum

$$q_\phi(\mathbf{z}^{(b)}) = \frac{1}{N} q_\phi(\mathbf{z}^{(b)} \mid \mathbf{x}^{(b)}) + \frac{1}{N} \sum_{\mathbf{x}^n \neq \mathbf{x}^{(b)}} q_\phi(\mathbf{z}^{(b)} \mid \mathbf{x}^n).$$

As also noted by Chen et al. [2018], the intuition behind this decomposition is that $q_\phi(\mathbf{z}^{(b)} \mid \mathbf{x}^{(b)})$ will in general be much larger than $q_\phi(\mathbf{z}^{(b)} \mid \mathbf{x}^n)$.

We can approximate the second term using a Monte Carlo estimate from samples $\mathbf{x}^{(b,c)} \sim q(\mathbf{x} \mid \mathbf{x} \neq \mathbf{x}^{(b)})$,

$$\frac{1}{N-1} \sum_{\mathbf{x}^n \neq \mathbf{x}^{(b)}} q_\phi(\mathbf{z}^{(b)} \mid \mathbf{x}^n) \simeq \frac{1}{C} \sum_{c=1}^C q_\phi(\mathbf{z}^{(b)} \mid \mathbf{x}^{(b,c)}).$$

Note here that we have written $1/(N-1)$ instead of $1/N$ in order to ensure that the sum defines an expected value over the distribution $q(\mathbf{x} \mid \mathbf{x} \neq \mathbf{x}^{(b)})$.

In practice, we can replace the samples $\mathbf{x}^{(b,c)}$ with the samples $b' \neq b$ from the original batch, which yields an estimator over $C = B - 1$ samples

$$\hat{q}(\mathbf{z}^{(b)}) = \frac{1}{N} q_\phi(\mathbf{z}^{(b)} \mid \mathbf{x}^{(b)}) + \frac{N-1}{N(B-1)} \sum_{b' \neq b} q_\phi(\mathbf{z}^{(b)} \mid \mathbf{x}^{(b')}).$$

Note that this estimator is unbiased, which is to say that

$$\mathbb{E}[\hat{q}(\mathbf{z}^{(b)})] = q(\mathbf{z}^{(b)}). \quad (18)$$

In order to compute the entropy, we now define an estimator $\hat{H}_\phi(\mathbf{z})$, which defines a upper bound on $H_\phi(\mathbf{z})$

$$\hat{H}_\phi[\mathbf{z}] \simeq -\frac{1}{B} \sum_{b=1}^B \log \hat{q}_\phi(\mathbf{z}^{(b)}) \geq H_\phi[\mathbf{z}]. \quad (19)$$

The upper bound relationship follows from Jensen's inequality which states that

$$\mathbb{E}[\log \hat{q}_\phi(\mathbf{z})] \leq \log \mathbb{E}[\hat{q}_\phi(\mathbf{z})] = \log q_\phi(\mathbf{z}). \quad (20)$$

B Model Architectures

We used two hidden variables for each of the datasets. One variable is modeled as a Normal distribution which represent style (denoted as z_n), and one modeled as a Concrete distribution to detect categories (denoted as z_c). We used Adam optimizer with learning rate $1e-3$ and default settings.

Encoder	Decoder
Input 28×28 grayscale image FC. 400 ReLU FC. 2×200 ReLU, FC. 10 (z_c) FC. 2×10 (z_n)	Input $z_n \in \mathbb{R}^{10}, z_c \in (0, 1)^{10}$ FC. 200 ReLU FC. 400 ReLU FC. 28×28 Sigmoid

Table 3: Encoder and Decoder architecture for MNIST and Fashion MNIST data.

Encoder	Decoder
Input 64×64 binary image FC. 1200 ReLU FC. 1200 ReLU FC. 2×400 ReLU, FC. 3 (z_c) FC. 2×10 (z_n)	Input $z_n \in \mathbb{R}^{10}, z_c \in (0, 1)^3$ FC. 400 Tanh FC. 1200 Tanh FC. 1200 Tanh FC. 64×64 Sigmoid

Table 4: Encoder and Decoder architecture for dSprite data.

Encoder	Decoder
Input 64×64 RGB image 4×4 conv, 32 BatchNorm ReLU, stride 2 4×4 conv, 32 BatchNorm ReLU, stride 2 4×4 conv, 64 BatchNorm ReLU, stride 2 4×4 conv, 64 BatchNorm ReLU, stride 2 FC. 2×256 ReLU, 2 FC. (z_c) FC. 2×20 ReLU	Input $z_n \in \mathbb{R}^{20}, z_c \in \{0, 1\}^2$ FC. 256 ReLU FC. $(4 \times 4 \times 64)$ Tanh 4×4 upconv, 64 BatchNorm ReLU, stride 2 4×4 upconv, 32 BatchNorm ReLU, stride 2 4×4 upconv, 32 BatchNorm ReLU, stride 2 4×4 upconv, 3, stride 2

Table 5: Encoder and Decoder architecture for CelebA data.

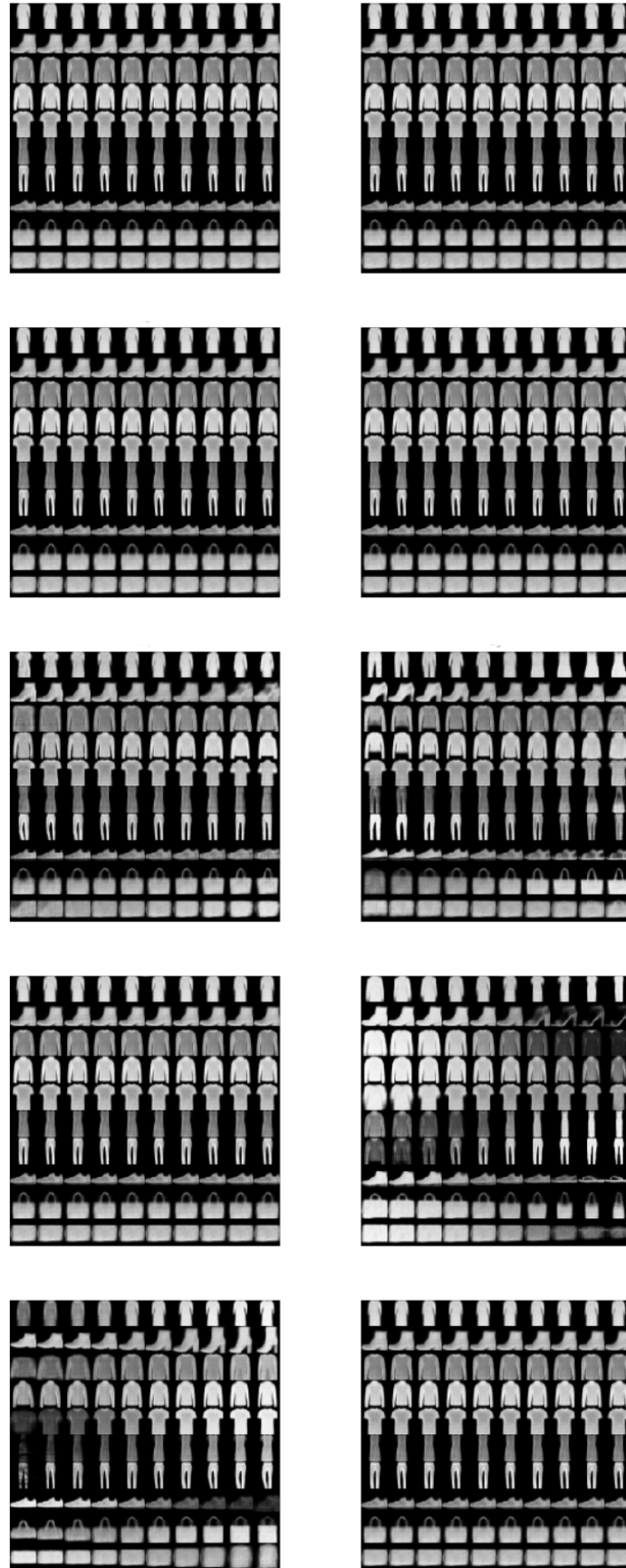


Figure 11: Qualitative results for disentanglement in Fashion-MNIST dataset. In each case, one particular z_d is varying from -3 to 3 while the others are fixed at 0.